Bulletin of the Seismological Society of America, Vol. 96, No. 4B, pp. S349–S363, September 2006, doi: 10.1785/0120050803

Seismic Evidence for Rock Damage and Healing on the San Andreas Fault Associated with the 2004 **M** 6.0 Parkfield Earthquake

by Yong-Gang Li, Po Chen, Elizabeth S. Cochran, John E. Vidale, and Thomas Burdette

Abstract We deployed a dense linear array of 45 seismometers across and along the San Andreas fault near Parkfield a week after the **M** 6.0 Parkfield earthquake on 28 September 2004 to record fault-zone seismic waves generated by aftershocks and explosions. Seismic stations and explosions were co-sited with our previous experiment conducted in 2002. The data from repeated shots detonated in the fall of 2002 and 3 months after the 2004 **M** 6.0 mainshock show ~1.0%–1.5% decreases in seismic-wave velocity within an ~200-m-wide zone along the fault strike and smaller changes (0.2%–0.5%) beyond this zone, most likely due to the coseismic damage of rocks during dynamic rupture in the 2004 **M** 6.0 earthquake. The width of the damage zone characterized by larger velocity changes is consistent with the low-velocity waveguide model on the San Andreas fault, near Parkfield, that we derived from fault-zone trapped waves (Li *et al.*, 2004). The damage zone is not symmetric but extends farther on the southwest side of the main fault trace. Waveform cross-correlations for repeated aftershocks in 21 clusters, with a total of ~130 events, located at different depths and distances from the array site show ~0.7%–1.1% increases in *S*-wave velocity within the fault zone in 3 months starting a week after the earthquake. The velocity recovery indicates that the damaged rock has been healing and regaining the strength through rigidity recovery with time, most likely due to the closure of cracks opened during the mainshock. We estimate that the net decrease in seismic velocities within the fault zone was at least ~2.5%, caused by the 2004 **M** 6.0 Parkfield earthquake. The healing rate was largest in the earlier stage of the postmainshock healing process. The magnitude of fault healing varies along the rupture zone, being slightly larger for the healing beneath Middle Mountain, correlating well with an area of large mapped slip. The fault healing is most prominent at depths above ~7 km.

Introduction

Extensive field and laboratory research and numerical simulations indicate that the fault zone undergoes high, fluctuating stress and pervasive cracking during an earthquake (e.g., Dieterich, 1978; Aki, 1984; Scholz, 1990; Rice, 1992; Kanamori, 1994). While we know slip is localized on faults because of their lower strength compared to the surrounding bedrock, critical parameters remain practically unknown (e.g., Sleep *et al.*, 2000). For example, the friction laws are approximate, and damage and healing rates are poorly constrained (e.g., Richardson and Marone, 1999; Morgan, 2004). Perhaps most critically, the magnitude of the strength reduction and its spatial extent has only been measured partially and at a few places before (e.g., Hickman and Evans, 1992; Vidale *et al.*, 1994). Earthquake-related fault-zone damage and healing have been documented quantitatively in only a few cases (e.g., Marone *et al.*, 1995; Li *et al.*, 1998, 2003; Massonnet *et al.*, 1996; Yasuhara *et al.*, 2005). In order to relate present-day crustal stresses and fault motions to the geological structures formed in their past earthquake histories, we must understand the evolution of fault systems on many spatial and time scales. Major crustal faults are structurally marked by zones of lowered velocity with a width of a few hundred meters to a few kilometers (Mooney and Ginzburg, 1986). Intense fracturing during earthquakes, brecciation, liquid-saturation, and possibly high pore-fluid pressure near the fault are thought to create these low-velocity zones. The size and magnitude of the low-velocity anomalies on active faults might vary over the earthquake cycle, as observed in our previous studies at rupture zones of the 1992 *M* 7.4 Landers and 1999 *M* 7.1 Hector Mine, California earthquakes (Li *et al.*, 1998, 2003; Li and Vidale, 2001; Vidale and Li, 2003).

Research at the San Andreas fault (SAF) at Parkfield has revealed a low-velocity zone a few hundred meters to 1 km

wide with velocity reductions of 10%–30% and a V_p/V_s ratio of 2.3 surrounding the surface trace of the SAF (e.g., Lees and Malin, 1990; Michelini and McEvilly, 1991; Eberhart-Phillips and Michael, 1993; Thurber *et al.*, 1997, 2003; Roecker *et al.*, 2004). The low V_s and corresponding high V_p/V_s ratios within the fault zone have been interpreted to be caused by dilatant fracturing due to high pore-fluid pressures. Magnetotelluric imaging of the SAF at Parkfield yields a similar model, with a zone of very low resistivity a few hundred meters wide extending to a depth of 3–4 km (Unsworth *et al.*, 1997); the low-resistivity zone is interpreted to be fluid rich. Byerlee (1990) and Rice (1992) suggest that pore fluids migrate up from depth and the fault-zone acts as a channel due in part to its greater permeability compared to adjacent blocks. Recent initial results from SAFOD drilling and borehole logs at Parkfield show a low-velocity zone with high porosity a couple of hundred meters wide at the ~3.2-km depth, indicating a damage zone associated with the SAF (Hickman *et al.*, 2005).

Fault-zone trapped-wave studies at Parkfield have shown a highly fractured zone characterized by a low-velocity waveguide on the SAF (Li *et al.*, 1990, 1997; Malin *et al.*, 2006; Shalev and Malin, 2005; Korneev *et al.*, 2003). We carried out an experiment at Parkfield in 2002 to record fault-zone trapped waves generated by near-surface explosions and microearthquakes within the fault zone, and used these waves to delineate a ~150-m-wide low-velocity zone in which seismic velocities are reduced by 25%–40% and seismic attenuation Q-values are ~20–50 along the fault strike at depths above 5 km (Li *et al.*, 2004). The data recorded after the 2004 **M** 6.0 Parkfield earthquake at our 2004 seismic array, co-sited with the experiment in 2002, provide better constraints on the depth extent of the damage structure on the SAF.

In this article, we report our observations of temporal changes in seismic velocity for repeated explosions detonated within the SAF on 16 October 2002 and on 28 December 2004 to document the coseismic damage associated with the 2004 **M** 6.0 Parkfield earthquake. In addition, results from repeated aftershocks recorded for 3 months starting a week after the mainshock confirm postmainshock healing of fault-zone rocks.

Data and Results

After the **M** 6.0 Parkfield earthquake on 28 September 2004, we deployed a dense seismic array of 45 PASSCAL three-channel RT130 seismometers across and along the SAF near the town of Parkfield to record aftershocks (Fig. 1a). The across-fault array A consisted of 35 stations with station spacing of 25 m, while array B and array C with station spacing 50 m were along the main SAF main trace and north strand. The array site was located in the middle of a high-slip part of the surface rupture in this earthquake and was co-sited with our experiment conducted at Parkfield in the fall of 2002. L22 2-Hz sensors were buried at the same locations as in the previous experiment. The three components of the sensor at each station were aligned vertical, parallel, and perpendicular to the fault trace. Coordinates of station ST0 of array A, located on the SAF main trace are 35°N 54.566′ and 116°W26.954′. Seismometers operated in a continuous mode, with sample rate at 100 samples per second. We recorded ~1000 aftershocks in 3 months, starting a week after the mainshock. On 28 December 2004, we detonated two near-surface explosions, each using ~250 kg of chemical explosives in a 30-m-deep hole drilled within the fault zone. The signals from shots were sampled at a rate of 500 samples per second. Shots PMM and WORK were located ~7 km northwest and ~9 km southeast of the array site. Shot PMM was a repeated explosion at the same shot-hole site in Middle Mountain as in our previous experiment in 2002. Coordinates of the shot-hole were 35°N57.481′ and 116°W30.237′. The clocks of all recorders and shot times were synchronized through the global positioning system (GPS). The timing errors for recorders and explosions were less than 2 msec. In the following part of this section, we show results from a quantitative analysis of the data from repeated shots and aftershocks to examine seismic velocity changes near the fault caused by this **M** 6.0 earthquake at Parkfield.

Repeated Shots

Figure 2a shows three-component seismograms recorded at array A across the SAF for shot PMM detonated on 28 December 2004. Fault-zone guided waves were dominant at stations close to the main fault trace, similar to those recorded at the same stations for this shot on 16 October 2002 (Li *et al.*, 2004). In Figure 2b, seismograms recorded for the repeated shots in 2002 and 2004 are overlaid with the shot times aligned at 0 sec. The first *P* arrivals at the wellhead geophone show identical travel times for repeated shots. However, traveltimes of *P, S*, and fault-zone guided waves at stations near the fault for the shot in 2004 were delayed by several tens of milliseconds. We measured the travel-time delays using waveform cross-correlation in three time windows including the *P, S*, and trapped waves, respectively, for each pair of recordings at the same recorder in 2002 and 2004. The length of the Hanning tapered time window is 0.5 sec for *P* waves, 1 sec for *S*, waves and 1.5 sec for guided waves. Figure 2c exhibits vertical-component seismograms recorded at three stations of array A for shots in 2002 and 2004. Cross-correlations of the waveforms in three time windows are shown in Figure 2d. Travel times of *P, S*, and guided waves to stations ST0 and E1 within the fault zone were delayed by 45, 80, and 120 msec in 2004, while travel times were delayed by 20, 35, and 50 msec at station W7 located 175m away from the fault, indicating larger velocity decreases within the fault zone. The measured changes in travel times are much larger than the uncertainty in the origin time of the explosion (a few milliseconds).

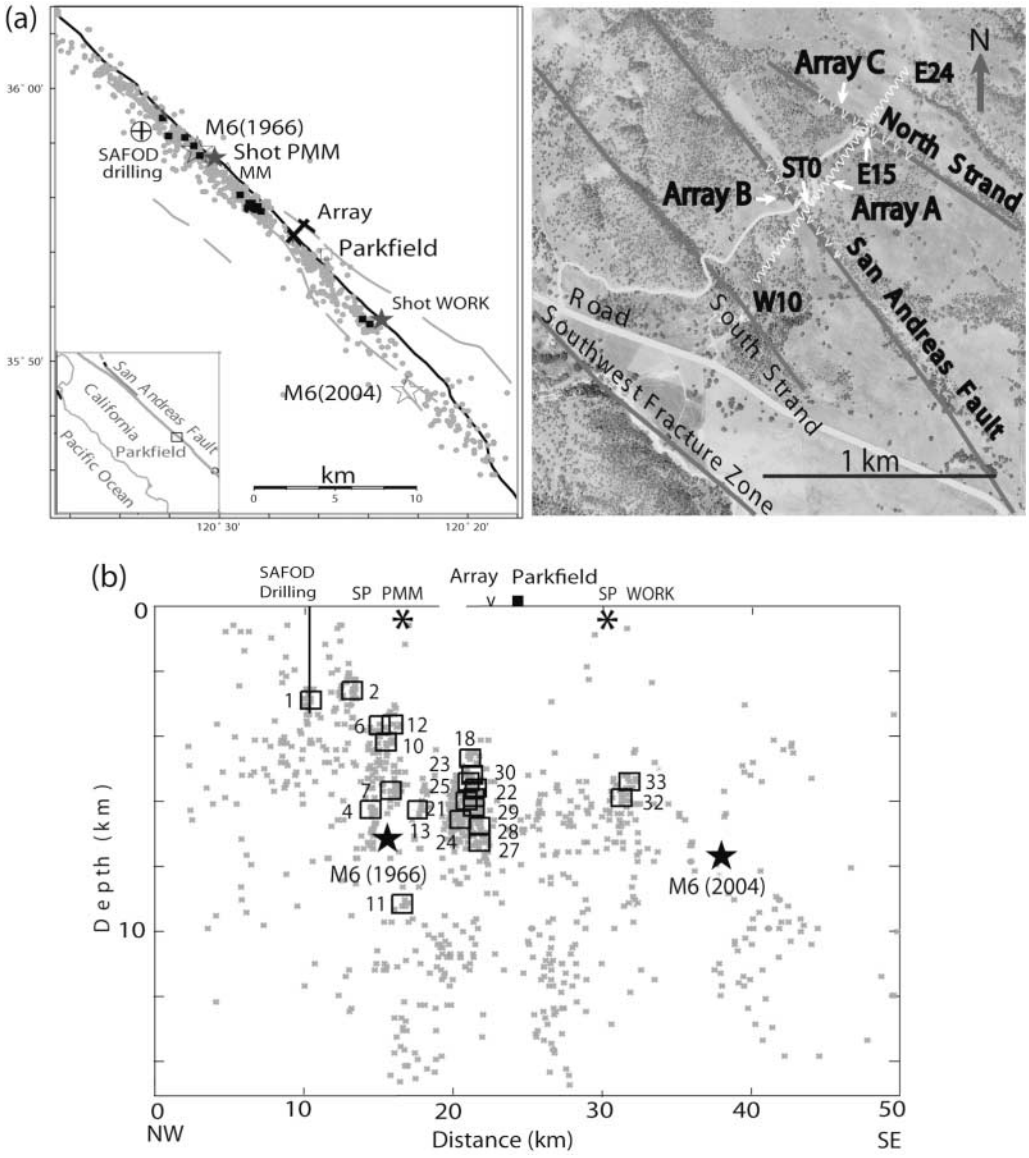

Figure 1. (a) Maps show locations of seismic array (denoted by bars), shots (solid stars) and aftershocks (dots) of the **M** 6.0 earthquake on 28 September 2004 at Parkfield, California. Seismic arrays were deployed across and along the San Andreas fault in 2002 and 2004. Solid squares denote clusters of repeated aftershocks used for this study. Array A consisted of 35 PASSCAL RT130s and 2-Hz L22 sensors with station spacing of 25 m. Arrays B and C consisted of 6 RT130s for each with station spacing of 50 m. Station ST0 was located on the main fault trace. Gray and white lines are fault surface traces and roads. Fault lines and topographic map are provided by Michael Rymer of the USGS. (b) The vertical section along the San Andreas fault at Parkfield shows locations of the seismic array, shots, the 1966 and 2004 **M** 6.0 earthquakes, and aftershocks in 2004. Twenty-one squares (labeled by numbers) denote clusters of repeated aftershocks; each cluster includes at least five similar aftershocks located within 200 m.

We applied the moving-window cross-correlation technique developed by Niu *et al.* (2003) based on the method used in coda-wave interferometry for estimating nonlinear behavior in seismic velocity (Snieder *et al.*, 2002) to measure the travel-time changes of seismic phases between the recordings from repeated shots. We examined low-pass (<3-Hz) filtered seismograms using a 1-sec window for cross-correlation, with the window center moving from the first *P* arrival to later *S* coda. To ensure reliable results from computations, we enforce a minimum correlation coefficient of 0.8 for the *P, S*, and guided waves. For example, Figure 2d shows moving-window cross-correlations of seismograms at three stations ST0, E1, and W7 of array A for shots in 2002 and 2004. The absolute travel-time delays in 2004 increase

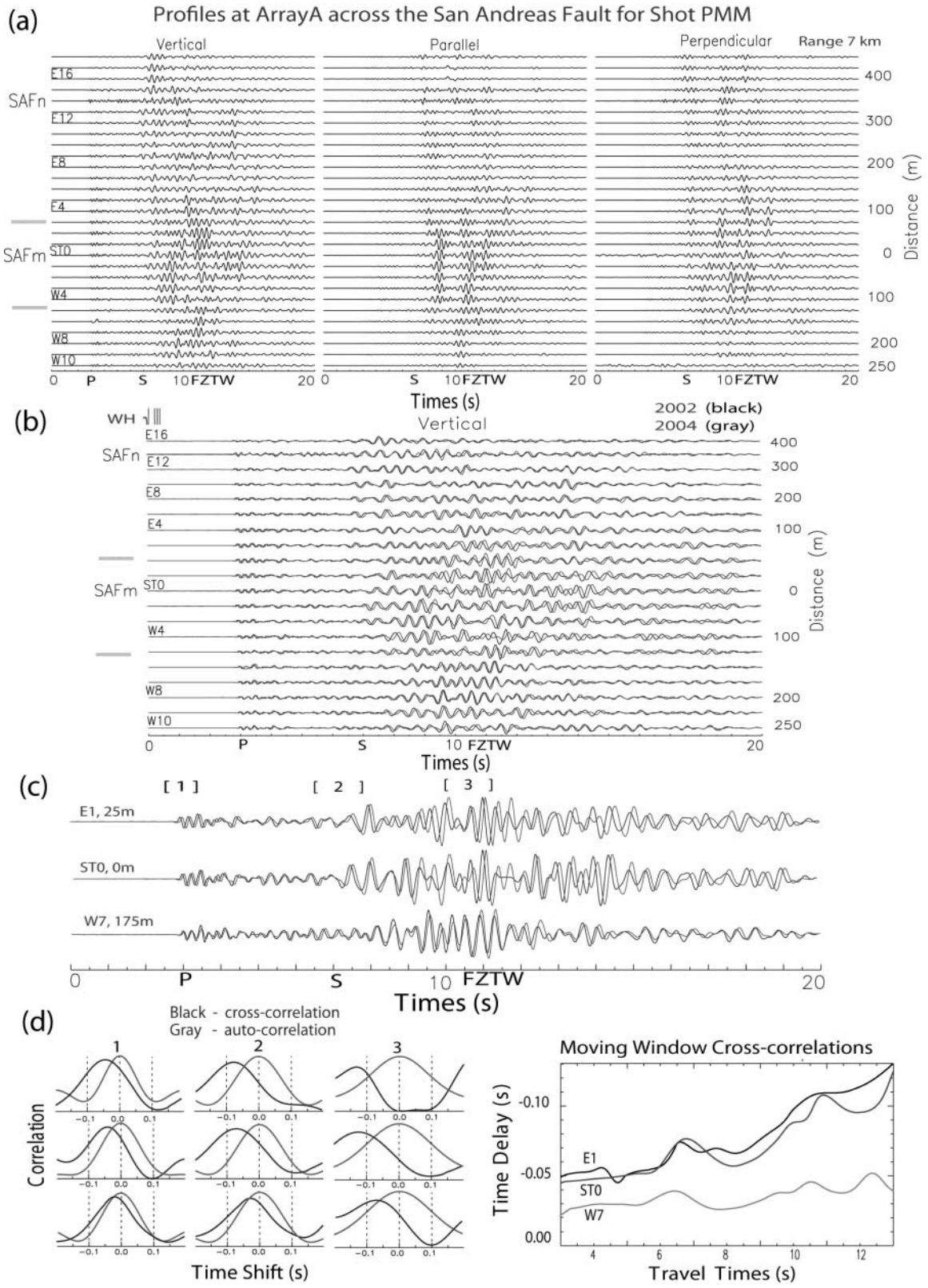
(a)
Profiles at ArrayA across the San Andreas Fault for Shot PMM
Vertical
Parallel
Perpendicular
Range 7 km
SAFn
SAFm
E16
E12
E8
E4
ST0
W4
W8
W10
400
300
200
100
0
100
200
250
Distance (m)
0 P S 10 FZTW 20
Times (s)
(b)
WH
Vertical
2002 (black)
2004 (gray)
SAFn
SAFm
E16
E12
E8
E4
ST0
W4
W8
W10
400
300
200
100
0
100
200
250
Distance (m)
0 P S 10 FZTW 20
Times (s)
(c)
[1]
[2]
[3]
E1, 25m
ST0, 0m
W7, 175m
0 P S 10 FZTW 20
Times (s)
(d)
Black - cross-correlation
Gray - auto-correlation
1
2
3
Correlation
−0.1 0.0 0.1
Time Shift (s)
Moving Window Cross-correlations
Time Delay (s)
-0.10
-0.05
0.00
E1
ST0
W7
4 6 8 10 12
Travel Times (s)

Figure 2. (a) Three-component seismograms recorded at array A across the San Andreas fault for shot PMM detonated at 7 km northwest of the array in 2004. Seismograms have been low-pass (<3-Hz) filtered and are plotted using a common scale for all traces in each plot. Station names and offsets from the fault are plotted. Stations ST0 and E15 were located on the main fault (SAFm) and north strand (SAFn). The shot origin time is at 0 sec. *P* and *S* waves arrive at ~3 sec and ~7 sec. Fault-zone trapped waves (FZTW) with large amplitudes and long wavetrains are dominant between *S* arrival and 15 sec at stations in the range of ~150 m marked by two bars. (b) Vertical-component seismograms at Array A for shot PMM in 2002 and 2004. Similar waveforms were recorded in repeated experiments, but waves traveled slower after the **M** 6.0 Parkfield earthquake in 2004. WH denotes the station located at the wellhead of shot-hole; the unclipped first *P* arrivals show identical arrival times for the repeated shots. (c) Vertical-component seismograms recorded at three stations within and out of the fault zone for shot PMM in 2002 and 2004. (d) Left: Autocorrelations (gray lines) of seismograms in 2004 and cross-correlations (black lines) of recordings at the same station in 2002 and 2004 for three time windows 1 to 3 including *P*, *S*, and trapped waves, respectively. The peak of the autocorrelation curve is at zero lag time in each window. The negative time shift indicates time advance. Greater time delays of waves in 2004 were registered at stations E1 and ST0 than at station W7. Right: Moving-window cross-correlations of waveforms at the three stations for shot PMM in 2002 and 2004 show time delays in 2004.

progressively for *P*, *S*, and guided waves, consistent with the measurements in the three time windows shown above.

Figure 3 shows results from array B along the main fault and array C along the north strand for repeated shot PMM in 2002 and 2004. Fault-zone guided waves with longer wavetrains follow *S* waves on array B than on array C (Fig. 3a). The overlaid seismograms recorded in 2002 and 2004 show clearly that waves traveled slower in 2004 (Fig. 3b), indicating seismic velocity decreases within the fault zone. Figure 3c shows overlaid seismograms and correlations of recordings in 2002 and 2004 at station N2 of array B and station N2 of array C. The measured travel-time delays for *P*, *S*, and guided waves in 2004 are 45, 85, and 125 msec on array B but are 25, 42, and 65 msec on array C, showing larger velocity decreases within the rupture zone along the main fault. In Figure 3d, we plot the percentage increase in travel times of *P*, *S*, and fault-zone guided waves at all stations on arrays A, B, and C for repeated shot PMM. Larger changes in travel times were observed at stations located closer to the fault trace in a range of ~200 m.

Assuming velocity changes were uniform in the crust sampled by these waves, the increases in travel time are straightforward to interpret. The *P* wave arrived with a 45-msec delay in 2004, with a travel time of ~3 sec, so the *P*-wave velocity decreased by ~1.5% within the fault zone between the fall of 2002 and 3 months after the **M** 6.0 earthquake in 2004. Similarly, the *S* wave arrived with an 85-msec delay in 2004, with travel time of ~6.8 sec, so the *S*-wave velocity decreased by ~1.25%. Trapped waves in window 3 with longer travel times had larger time advances than did *P* and *S* waves, again resulting in ~1.25% increase in velocity within the rupture zone. In contrast, the *S*-wave velocity decreased by ~0.5% in the surrounding rocks. Based on the width of the zone exhibiting larger travel-time increases between 2002 and 2004, we estimate that the zone that experienced fracturing and damage during the **M** 6.0 mainshock is about ~150–200 m wide in the top few kilometers. The width of this zone is consistent with the low-velocity waveguide on the SAF delineated using fault-zone trapped waves at the same array site in our previous experiment at Parkfield in 2002 (Li *et al.*, 2004), suggesting the width of the fault zone is stable while velocities within it change over time. We will examine in greater detail the width of the low-velocity waveguide after the 2004 **M** 6.0 event using guided waves in a future study. Assuming that there was no significant change in seismic velocity between 16 October 2002 and 28 September 2004 in the Parkfield region, the measured velocity decreases between 2002 and 2004 are most likely caused by the coseismic rock damage, with cracks opening due to the latest **M** 6.0 Parkfield earthquake. Although processes associated with aseismic transients have shown to influence wave propagation (Niu *et al.*, 2003), there were no such transients and resolvable measurements in seismic velocity in the Parkfield area during this time period (Rubinstein and Beroza, 2005). We note that the damage zone is not symmetric with the main fault trace but is broader on the southwest side. Also note that the velocity decreases on the north fault strand were smaller than those within the damage zone on the main fault, but larger than the background velocity changes in surrounding rocks. In our previous study of fault-zone structure at Parkfield, we delineated a distinct low-velocity waveguide on the main fault and a waveguide with smaller velocity reduction on the north strand at this site. The north strand might have experienced minor breaks due to secondary slip and strong shaking from ruptures on the main fault in the 2004 **M** 6.0 earthquake.

The observed velocity decrease within the fault zone may be interpreted as dilatancy (Nur, 1972). Estimates of the change in velocity due to the change in the density of cracks may be calculated using equations in which the elastic constants of fractured rock are functions of the crack density (O'Connell and Budiansky, 1974). We assume randomly oriented cracks and compute the change in apparent crack density from measured changes in seismic velocity. The apparent crack density is defined by $\varepsilon = N(a^3)/V$, where a is the radius of the flat penny-shaped crack, and N is the number of cracks in a volume V. We assume cracks to be partially water filled and estimate that Poisson's ratio is 0.33. For the calculation, we use an average $V_p = 3.0$ km/sec and $V_s = 1.5$ km/sec for the fault-zone rocks at depths above ~5 km (Li *et al.*, 2004). Calculations reveal that the apparent crack density within the fault zone increased by ~0.018 in accordance with ~1.25% decrease in *S* velocity due to ~2.5%

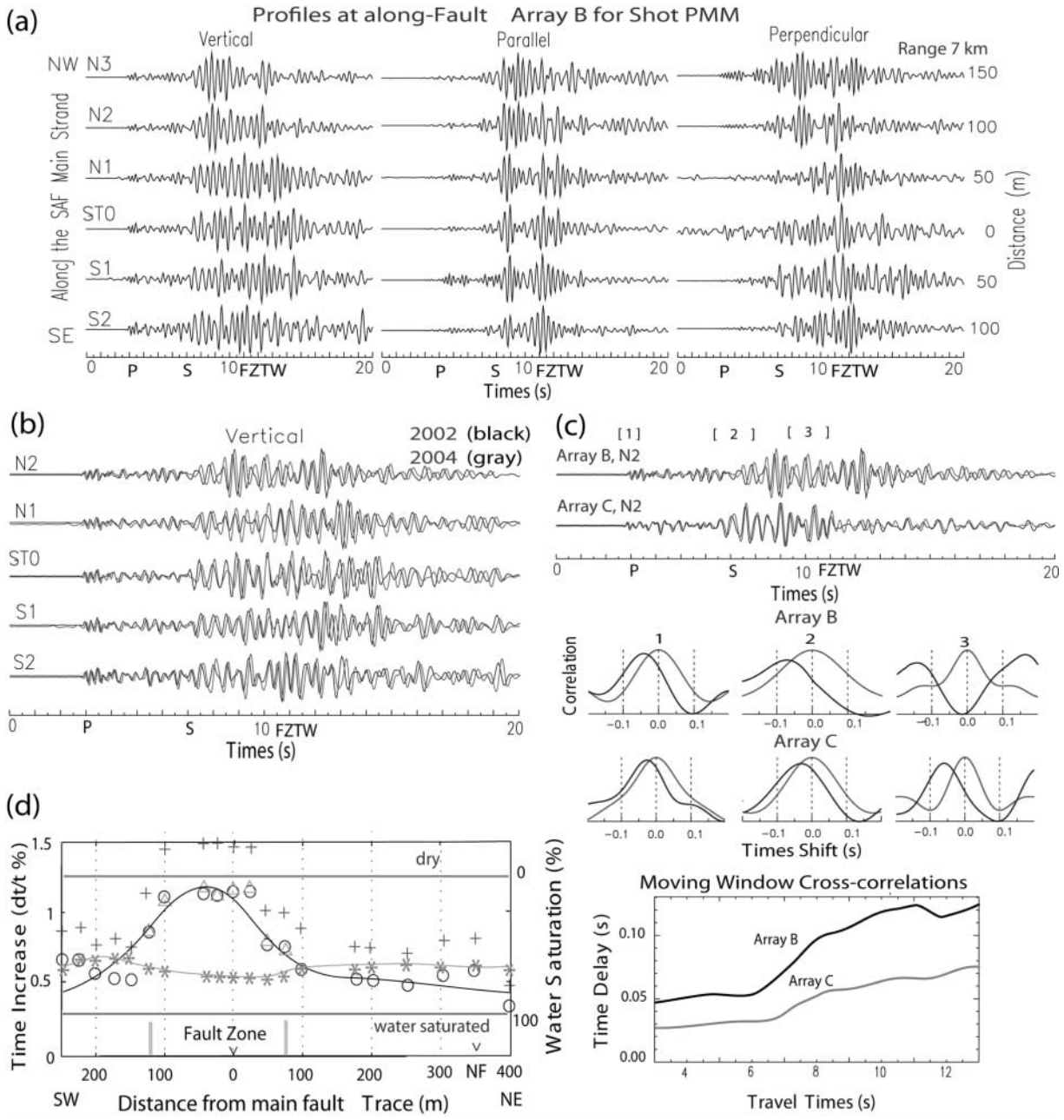

Figure 3. (a) Three-component seismograms recorded at array B along the main trace of San Andreas fault for shot PMM in 2004. Seismograms have been <3-Hz filtered and are trace-normalized in plot. Station names and distances from station ST0 are plotted. Other notations are the same as in Figure 2. (b) Overlapped seismograms recorded at Array B for repeated shot PMM in 2002 and 2004 show similar waveforms, but waves traveled slower after the 2004 **M** 6.0 Parkfield earthquake. (c) Vertical-component seismograms recorded at station N2 of array B and station N2 of array C for repeated shot PMM. Cross-correlations of recordings in 2002 and 2004 for time windows 1 to 3 including *P*, *S*, and trapped waves (top) and for moving-window show travel-time delays in 2004, with larger delays at array B along the main fault than those at array C along the north strand. (d) Travel-time increases, in percent, for *P* (crosses), *S* (circles), and trapped waves (triangles) measured from cross-correlations of seismograms at array A across the SAF for repeated shot PMM in 2002 and 2004, showing that seismic velocities decreased after the 2004 **M** 6.0 earthquake due to rock damage within the fault zone. Some stations did not work in both experiments due to weather and battery problem. The black line is a polynomial fit to travel-time increases of *S* waves in 2004. A pair of vertical gray bars denotes a zone with greater travel-time increases. Ratio of travel-time changes for *P* waves to *S* waves (gray stars with a curve) indicate the degree of water saturation in cracks. Two horizontal light lines indicate the ratios predicted for a range of water percentage for a Poisson solid. NF, north fault strand.

decrease in shear rigidity of the fault-zone rock during the time period between two repeated shots.

If observed changes in seismic velocity are modeled by fluid-filled cracks, then the degree of fluid saturation in cracks can be estimated from the ratio of changes in travel time of *P* waves to *S* waves ($\Delta t_p/\Delta t_s$) because *S*-wave velocity does not depend as strongly as *P*-wave velocity on the amount of water in cracks. We have estimated water saturation degrees within low-velocity zones along ruptures in the 1992 Landers and 1999 Hector Mine earthquakes using this method (Li *et al.*, 1998, 2003). According to equations for the elastic moduli of the medium with isotropically oriented penny-shaped cracks (Garbin and Knopoff, 1975), the ratio of travel-time changes of *P* to *S* waves ($\Delta t_p/\Delta t_s$) in a Poisson solid is ~1.22 for dry cracks and ~0.27 for water-saturated cracks (Li *et al.*, 2003). More precisely, in our study area where the *P*-wave velocity is about twice the *S*-wave velocity, the rock has an anomalous Poisson's ratio of 0.33 (see details in the discussion section). In this medium, $\Delta t_p/\Delta t_s$ is predicted to be 1.64 for dry cracks and 0.17 for water-saturated cracks. Figure 3d shows the $\Delta t_p/\Delta t_s$ values at array A across the SAF for repeated shot PMM in 2002 and 2004. The value of $\Delta t_p/\Delta t_s$ is ~0.57 within the fault zone and ~0.65 out of the zone, indicating more water included in cracks within the fault zone at shallow depth. The initial saturation degree of water in cracks before the mainshock is not predicted because no travel-time changes for *P* to *S* waves ($\Delta t_p/\Delta t_s$) before the 2004 **M** 6.0 earthquake are available.

Repeated Aftershocks

Using the catalog of Northern California Seismic Network (R. M. Nadeau, personal comm., 2005), we selected 21 clusters of repeated aftershocks among ~1000 aftershocks recorded at our seismic array in 3 months starting a week after the 2004 **M** 6.0 earthquake. Each cluster includes at least five repeated aftershocks occurring at the same place, with the location difference among them smaller than 200 m and the difference in magnitude smaller than 0.5. The location precision of Parkfield earthquakes in the catalog is less than a few tens of meters in relative distance. The repeated aftershocks in each cluster show similar waveforms with correlation coefficient higher than 0.8. We found a total of about ~130 such repeated aftershocks in 21 clusters located at depths between ~3 km and ~9 km along the ~25-km-long rupture zone of the 2004 **M** 6.0 earthquake (Fig. 1b). We examined these repeated aftershocks to determine seismic velocity changes with time after the mainshock. It is noted that we lack of data in the first week after the mainshock.

For example, Figure 4a–c shows similar seismograms recorded at array A across the SAF for a pair of repeated aftershocks in cluster 28 at 6.9 km depth and 2 km northwest of the array site, occurring on 4 November and 3 December 2004. Prominent fault-zone guided waves with long-duration wavetrains appeared at stations close to the main fault trace in a width range of ~150 m. The time-expanded seismograms in Figure 4b show that seismic waves from the later event traveled faster than those from the earlier event with larger travel-time advances at station STO on the main fault than those at station W8, 200 m away from the fault. Waveform cross-correlations show that travel-time advances of *S* and guided waves from the later aftershock arriving at station ST0 are 25 msec and 38 msec plus the undetermined change in *P* travel time, but much smaller at station W8. These observations indicate that the fault zone has been healing such that the rigidity recovers with time, most likely due to the closure of cracks that opened in the **M** 6.0 earthquake. In Figure 4c, we display seismograms at five stations of array A for a pair of repeated aftershocks in cluster 24 at 6.4 km depth and ~2 km northwest of the array, occurring on 9 and 29 October. Note that fault-zone guided waves show longer wavetrains after *S* waves at stations within the rupture zone than those farther away from the fault. Waveform cross-correlations exhibit travel-time advances for the later event, with larger changes at stations within the rupture zone. The moving-window cross-correlation of seismograms at station ST0 for repeated aftershocks shows progressive increase in travel-time advance from 32 msec to 55 msec for *S* and guided waves, reflecting that seismic velocities have increased within the fault zone after the mainshock. Travel-time advances of seismic waves between 9 and 29 October measured in this example are larger than those between 4 November and 3 December, shown in Figure 4b, although the time span between repeated events in each example and the travel distance from these events are similar (Fig. 1b), indicating that seismic velocities increased more rapidly in the earliest stage after the mainshock.

The trend of healing rate decreasing with time is shown in more detail by the examples given below. Figure 5a exhibits seismograms recorded at station W4 of array A for four repeated aftershocks in cluster 29 at 6.5 km depth and ~2 km northwest of the array, showing very similar waveforms, with the correlation coefficient higher than 0.9 (Fig. 5a). Travel-time advances measured by moving-window cross-correlation for the first pair of repeated events occurring on 7 October and 7 November are ~30–50 msec for *S* and guided waves in travel time plus the change in *P* travel time, nearly twice as large as those for the second pair of repeated events occurring on 28 November and 26 December. Figure 5b exhibits seismograms and moving-window cross-correlations of waveforms recorded at station W4 for four repeated aftershocks in cluster 28, occurring on 10 October, 4 November, and 3 and 17 December 2004. The relative decreases in travel time for these waves were measured to be ~30–50 msec in the first month, ~20–30 msec in the second month, and less than ~15 msec in the third month after the mainshock, indicating that the postseismic fault-healing rate is not constant but decreased with time. The healing is still observable 3 months after the mainshock, but the healing rate reduced to a third of that seen in the first month.

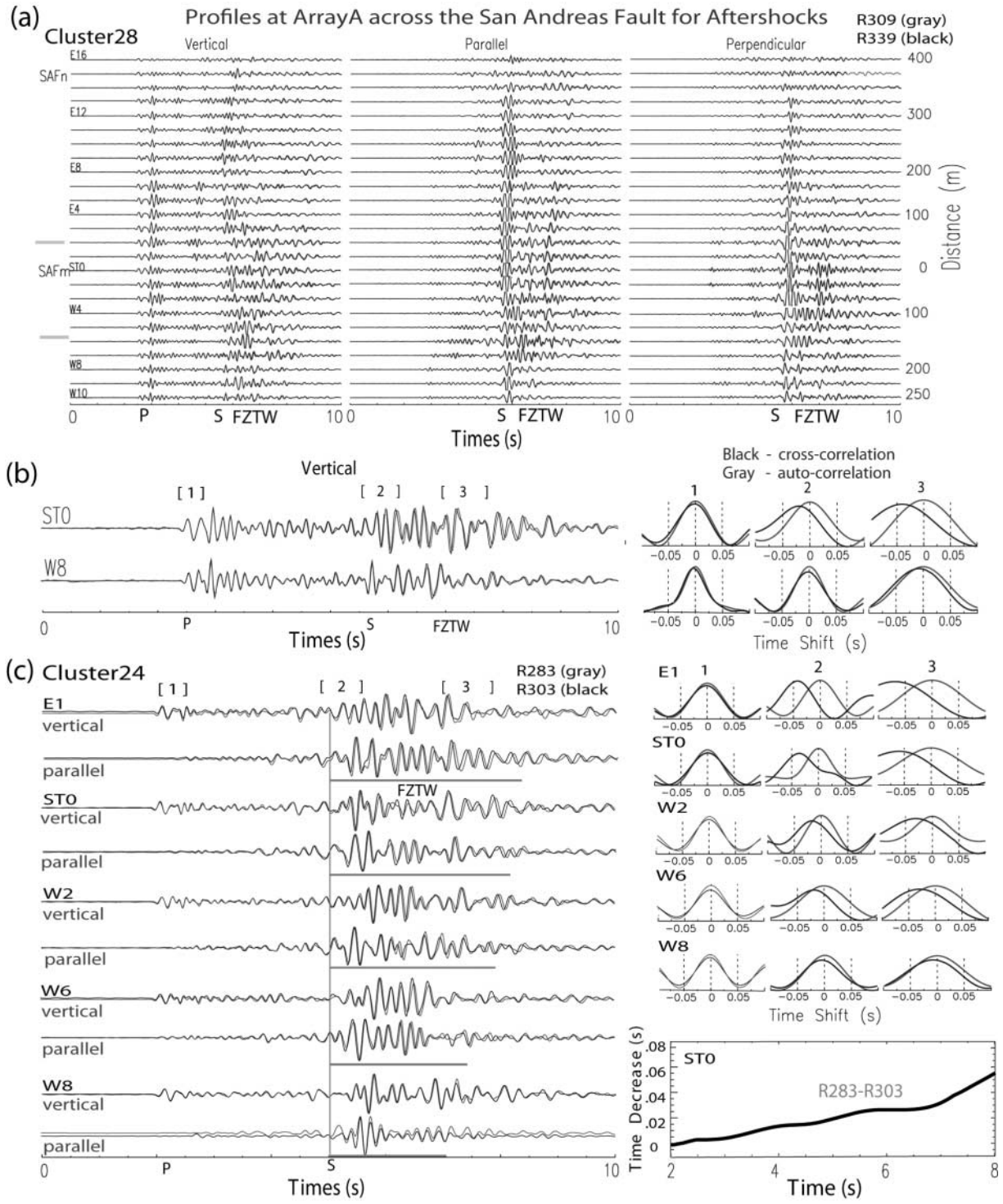

Figure 4. (a) Three-component seismograms recorded at array A across the SAF for two repeated aftershocks in cluster 28, occurring on 4 November (Julian date R309) and on 3 December (R339) 2004. Seismograms have been low-pass (<8-Hz) filtered and are trace-normalized in plot. Similar waveforms were recorded at array A for repeated aftershocks. Other notations are the same as in Figure 2. (b) Overlaid seismograms and waveform cross-correlations at stations ST0 and W8 located within and 200 m away from the fault for the repeated aftershocks. The first *P* arrivals for two events are aligned at the same time in the plot. *S* waves from the later event travel faster than the early event, with much larger time advance within the fault zone, indicating that the fault has been healing with rigidity recovery after the **M** 6.0 mainshock. (c) Overlapped vertical and parallel-to-fault component seismograms at five stations of array A for two repeated aftershocks in cluster 24 occurring on 9 (R283) and 29 (R303) October 2004. The first *P* arrivals for two events are aligned at the same time in plot. Horizontal bars denote the length of fault-zone-trapped wavetrains, showing longer trapped wavetrains following *S* waves at stations within the fault zone. Cross-correlations of vertical-component seismograms in three time windows at five stations, and moving-window cross-correlation of waveforms at station ST0 for two repeated aftershocks show that waves traveled faster for the later event and with larger advances at stations within the fault zone.

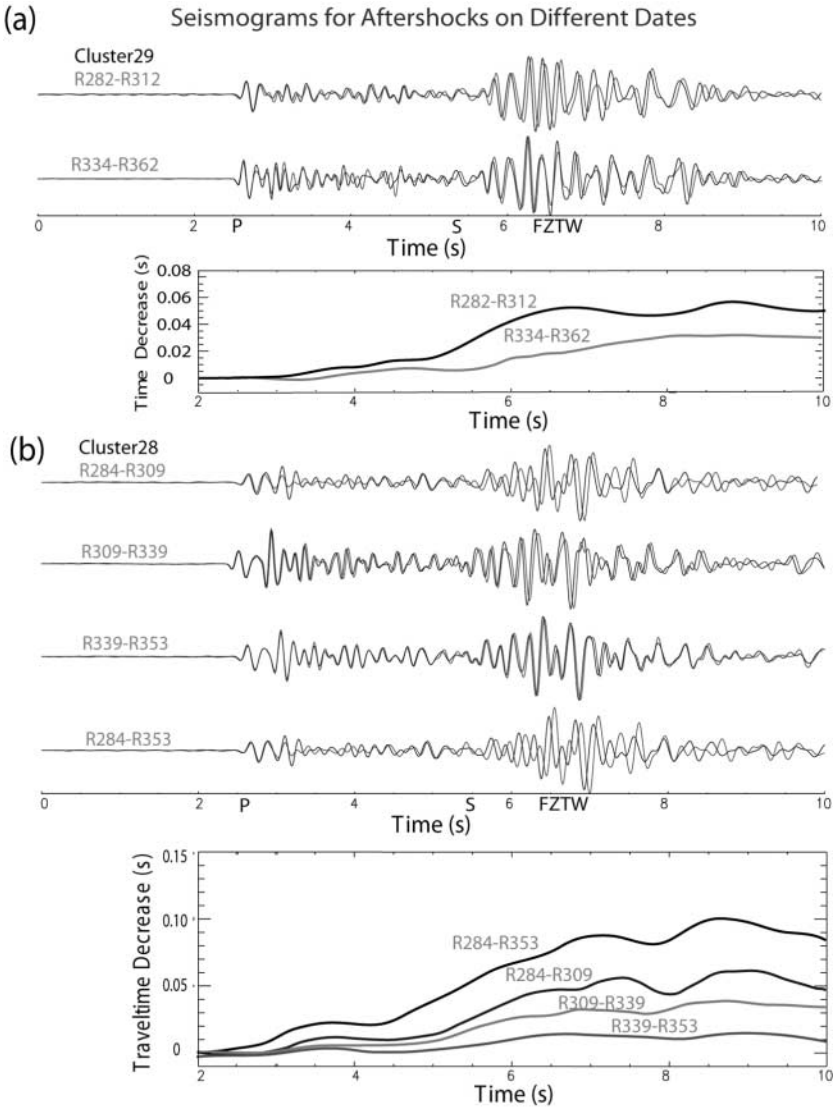

Figure 5. (a) Vertical-component seismograms recorded at station W4 of array A for four repeated aftershocks in cluster 29, occurring on 7 October (R282), 7 November (R312), 28 November (R334), and 26 December (R362) 2004. Seismograms have been low-pass (<8-Hz) filtered and are plotted in gray and black lines for the earlier and later events in each pair. Moving-window cross-correlations of waveforms show that the travel-time advance in the first pair of repeated aftershocks is larger than that in the second pair of aftershocks. The time spans in the two pairs are the same, indicating that the healing rate was larger in the earlier stage after the mainshock. (b) Same results from a sequence of four repeated aftershocks in cluster 28, occurring on 10 October (R284), 4 November (R309), 3 December (R339), and 17 December (R353), show greater travel-time advance in the earlier stage of the postseismic fault-healing process.

The following examples show variations in travel-time change across the fault zone. Figure 6a exhibits seismograms recorded at four stations of array A for two repeated aftershocks in cluster 6 at 3.9 km depth and ~8 km northwest of the array site, occurring on 15 October and 16 November 2004. Moving-window cross-correlations show an advance of ~40–55 ms in travel times of *S* and guided waves to stations ST0 and W2 within the fault zone, larger than those (~10–20 msec) to stations E6 and E7 located at 150–175 m northeast of the fault. In Figure 6b, we display the relative changes in travel time of *S* waves and guided waves at all available stations of array A measured by moving-window cross-correlations for these two repeated aftershocks, showing larger travel-time decrease at stations within the fault zone. Figure 6c illustrates the travel-time changes, in percent, for *S* and guided waves at all working stations of array A for six repeated aftershocks in cluster 6 occurring between 15 October and 15 December 2004. Travel times for *S* and guided waves decreased by ~1.1% within the rupture zone in this time period, but with a smaller change (~0.5%) out of the zone. Note that the travel-time decreases at stations near the north fault strand were slightly larger than the background level in surrounding rocks. These observations indicate that the rocks damaged in the 2004 **M** 6.0 earthquake have been healing with larger healing magnitude within the rupture zone than in surrounding rocks.

We then examined the data for variations in travel-time change along the fault strike and with depth. Figure 7a exhibits the seismograms recorded at station W4 of array A for two repeated aftershocks in cluster 18 occurring at 4.6 km depth on 11 October and 8 December, and two repeated events in cluster 11 occurring at 9.2 km depth on 14 October and 5 December. Moving-window waveform cross-correlations show that travel-times of *S* and guided waves were decreased by ~50–80 msec, plus changes in *P* waves for the pair of deeper repeated aftershocks, but by ~30–50 msec for the pair of shallower events, although the time span of repeated events in the two pairs is nearly the same. In Figure

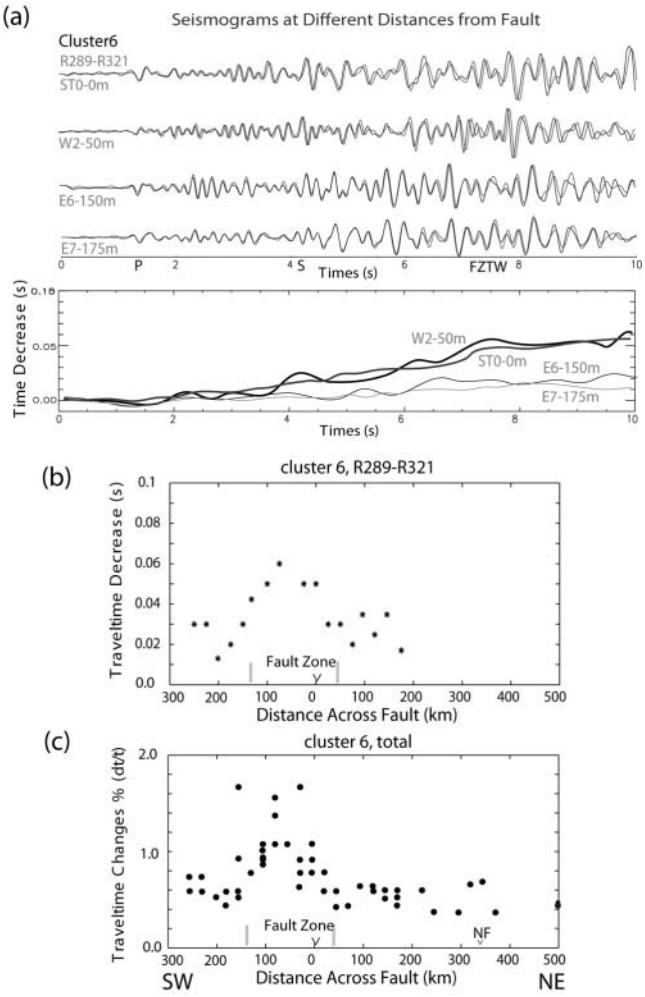

Figure 6. (a) Vertical-component seismograms recorded at four stations of array A for two repeated aftershocks in cluster 6, occurring on 15 October (R289) and 16 November (R3210). Other notations are the same as in Figure 5. Moving-window cross-correlations show that travel-time advances are larger at stations close to the fault and much smaller at stations located 150–175 m east of the fault. (b) Travel-time decreases of *S* waves measured by waveform cross-correlations at array A for these two repeated aftershocks show larger travel-time advances within the fault zone in a width range of ~200 m, indicating the larger healing rate in the rupture zone where the rock experienced greater damage in the 2004 **M** 6.0 earthquake. Note that this zone is not symmetric with the main fault trace, but broader on the southwest side of the main fault trace. (c) Travel-time advances, in percent, for *S* waves measured from waveform cross-correlations at array A for all available pairs of six repeated aftershocks in cluster 6, occurring on Julian dates 289, 299, 308, 321, 332, and 354 in 2004. The data have been adjusted for changes in travel times for *P* waves in a Poisson's solid. Results show larger travel-time advance (velocity increase) after the mainshock within the fault zone. The measurements of travel times for each pair of repeated aftershocks have been normalized to a time period of 20 days. NF, the north fault strand.

7b, we show seismograms recorded at station W4 for two repeated aftershocks in cluster 12 occurring at 3.7 km depth on 7 October and 29 November, and another two repeated aftershocks in cluster 4 at 6.5 km on 13 October and 20 November. Again, we see larger travel-time decreases for the pair of deeper repeated events. These observations suggest that the postmainshock healing occurred on the ruptured fault to a depth of at least 6–7 km, probably across the seismogenic depths but with smaller healing magnitude in the deeper portion of the fault zone. The increasing pressure with increasing depth will reduce the crack density and probably increase the rate of healing of damage caused by earthquakes. It is also likely to influence the development of fault gouge (Scholz, 1990; Marone, 1998) and the mineralogy of the rocks (Angevine *et al.*, 1982). Thus, the fault-zone properties are dependent on depth.

In summary, Figure 8 shows relative decreases in travel time for *S* and guided waves at nine stations between W5 and E3 located in a range of 200 m across the fault for 226 pairs of repeated aftershocks in 21 clusters measured by an automatic computer procedure for moving-window cross-correlation. The catalog includes more pairs of repeated aftershocks in the 21 clusters, but parts of them were not recorded at some stations of array A because of battery problems. Also, some repeated aftershocks with correlation coefficients lower than 0.7 are not used for computation. We used the data from repeated aftershocks with the first event occurring before 26 October (R300) and the second event occurring at least 20 days after the first event in the pair. The measured decreases in travel time for pairs with longer time span between repeated aftershocks are normalized to the change in 20 days. Figure 8a shows measured relative travel-time decreases for *S* waves from these repeated aftershocks as a function of position along the fault strike. Although the data are scattered, the repeated aftershocks in group one located close to the hypocenter of the **M** 6.0 earthquake in 1966 beneath Middle Mountain show relatively large changes in travel time, although the average depths of the three groups of clustered aftershocks used in this plot are nearly the same. Langbein *et al.* (2005) surveyed surface rupture and postmainshock surface slip after the 2004 28 September **M** 6.0 Parkfield earthquake. They found the greatest dextral slip of 44 mm in the Middle Mountain area. The preliminary results from inverse of GPS and broadband waveform data show the maximum slips of ~0.6 m at depths of 4–6 km beneath Middle Mountain. Figure 8b shows travel-time decrease for these repeated aftershocks versus event depths. We see an increasing trend of cumulative travel-time changes as the depth increases from 3 km to 7 km, although the data are scattered.

Discussion and Conclusion

Our seismic study at Parkfield indicates that the active fault zone, which undergoes strong dynamic stresses and pervasive cracking during a major earthquake, has a distinct

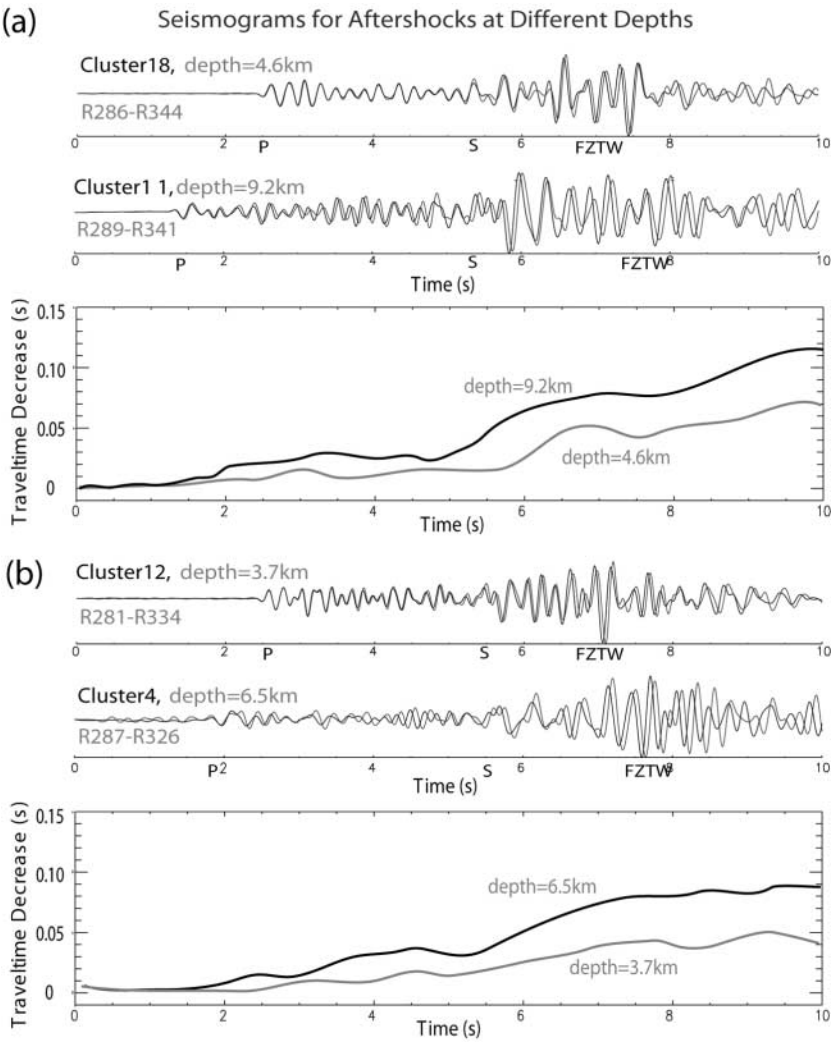

Figure 7. (a) Vertical-component seismograms recorded at station W4 of array A for two repeated aftershocks in cluster 18 at 4.6 km depth and another two repeated events in cluster 11 at 9.2 km depth. Other notations are the same as in Figure 5. Moving-window waveform cross-correlations show that the travel-time decreases for the pair of deeper aftershocks are larger than those for the pair of shallower events, although time spans between the repeated events in two pairs are nearly the same. (b) Vertical-component seismograms and moving-window waveform cross-correlations at station W4 of array A for two repeated aftershocks in cluster 12 at 3.7 km depth and another two repeated events in cluster 4 at 6.5 km depth, showing larger travel-time decreases for the pair of deeper aftershocks. These observations suggest that the healing occurred on the SAF, likely across seismic depths to ~9 km, although with smaller healing magnitude within the deeper portion of the fault zone.

low-velocity zone that coseismically weakens and consequently heals. We have used fault-zone trapped waves to delineate a ~150-m-wide low-velocity damage zone on the SAF at Parkfield, in which seismic velocities are reduced by 25%–40% from wall-rock velocities (Li *et al.*, 2004). Although this damage zone along the fault strike has accumulated over geological time, it was in part weakened by the latest **M** 6.0 Parkfield earthquake in 2004, possibly due to inelastic deformation around the propagating crack tip in the 2004 **M** 6.0 mainshock, as predicted by existing fault-zone rupture models (e.g., Rice, 1980; Scholz, 1990).

The data acquired in our recent experiments at Parkfield provide details of coseismic damage and postmainshock healing on the SAF associated with the 2004 **M** 6.0 earthquake. In summary, Figure 9a shows seismic velocity changes measured at our seismic arrays deployed at Parkfield before and after this earthquake. Our measurements for repeated shots on 16 October 2002 and 30 December 2004 show a decrease of ~1.25% in shear-wave velocity within the fault zone, most likely due to rock damage, with crack opening caused by dynamic rupture in the **M** 6.0 earthquake on 28 September 2004, assuming that there was no significant change in seismic velocity at Parkfield area in the time period between the shot in 2002 and the 2004 **M** 6.0 earthquake (Rubinstein and Beroza, 2005). The water table change will affect the seismic velocity at shallow depth. As we carried out repeated experiments in the fall of 2002 and 2004, there would not have been significant variations in water table at that time at Parkfield. It is reasonable to attribute the observed velocity changes to the 2004 **M** 6.0 event. Measurements for repeated aftershocks show the velocity increased by ~1.1% within the rupture zone during 3 months starting a week after the mainshock, reflecting the healing of the damaged rocks most likely due to the closure of cracks that had opened during the latest **M** 6.0 Parkfield earthquake, in 2004. The healing rate is not constant but decreases with time (Fig. 5). It suggests that a fault may regain strength rapidly in the early stage in the postmainshock period but may take a reasonable long time to fully recover its strength for the next earthquake.

Healing varies across the fault zone, with greatest healing occurring within a ~200-m-wide zone (Fig. 6) that ex-

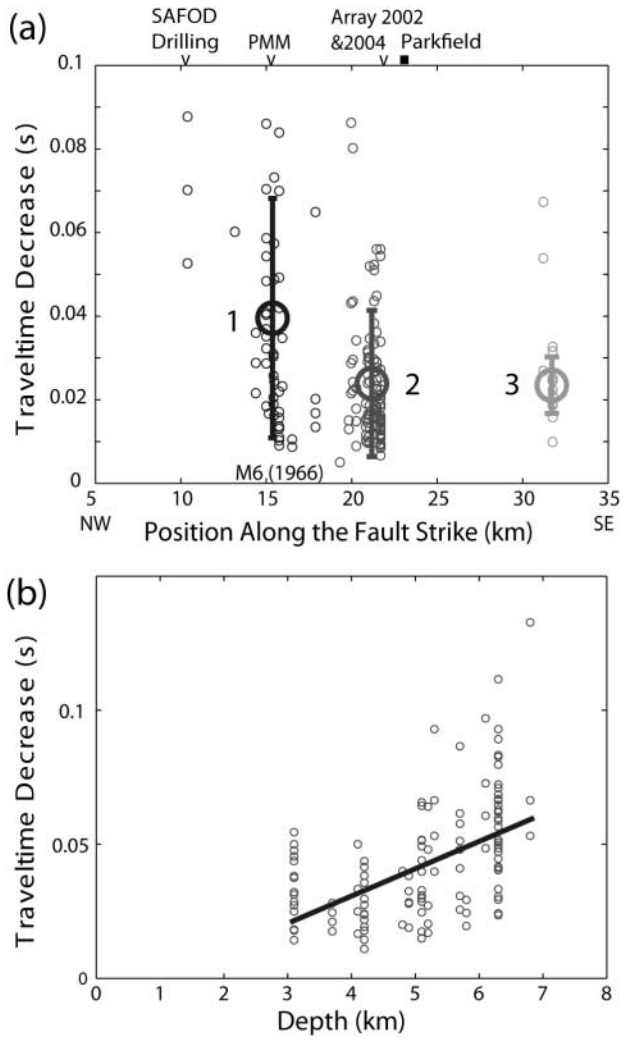

Figure 8. Travel-time decreases measured at nine stations W5–E3 located within the fault zone for 226 pairs of repeated aftershocks in 21 clusters, with the first event in each pair occurring before 26 October (R300) and the second event occurring at least 20 days later than the first event. The measured time decreases for each pair of repeated aftershocks have been normalized to the changes in 20 days. The mean values and standard deviations of the data for three groups of clusters labeled 1, 2, and 3 are marked by large circles and error bars. Group 1 is located close to the hypocenter of the 1966 **M** 6.0 earthquake. The data have been normalized to a depth range of 4 km to remove the effect of different depths of pairs on measurements. Aftershocks in group 1 occurring on or close to the slip patch of the **M** 6.0 earthquake in 1966 show larger travel-time decreases, although three groups of clusters are nearly at the same average depth. (b) The data used in (a) are plotted versus depths of repeated aftershocks. The straight line is the least squares fit to the data, showing that the accumulated travel-time advance increases as the event depth increases between depths of 3 km and 7 km. The results suggest that the fault experienced healing after the 2004 **M** 6.0 Parkfield earthquake at seismogenic depths to ~7 km, although the magnitude of healing is smaller in the deeper portion of fault zone.

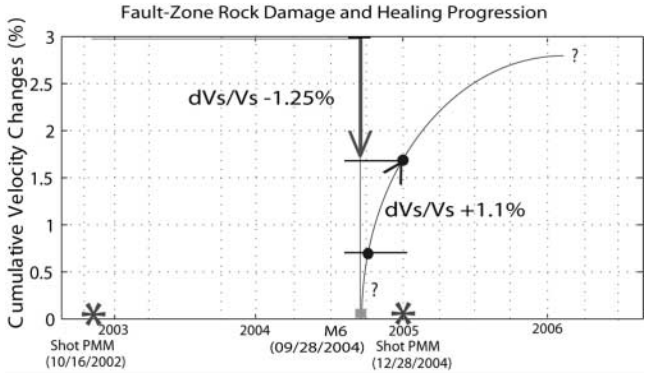

Figure 9. *S*-wave velocity changes within the rupture zone on the SAF associated with the **M** 6.0 Parkfield earthquake on 28 September 2004. The *S* velocity decreased by ~1.25% in the time period between the two repeated shots on 16 October 2002 and 28 December 2004, most likely due to the coseismic rock damage during this **M** 6.0 mainshock. The velocity within the rupture zone then increased by ~1.1% in 3 months starting a week after the mainshock, showing postmainshock fault healing with rigidity recovery of damaged rocks within the fault zone. The healing rate is not constant but decreases with time, although details just after the existing data and extrapolation into the future are not well constrained. The velocity changes in the first week after the mainshock were not measured in this study.

perienced greater damage in the mainshock. This damage zone is asymmetric, broader on the southwest side of the main fault trace. The asymmetry may imply that the fault zone has a significant cumulative damage due to previous large earthquakes on the SAF. When a fault ruptures, it may preferentially damage the already-weakened rocks in the zone, even though those rocks are not symmetrically distributed on either side of the main slip plane (Chester *et al.*, 1993). Recent results from the SAFOD drilling project and borehole logs at Parkfield show high porosity and multiple slip planes in an ~200-m-wide low-velocity zone, with velocity reduction of ~25% on the SAF at ~3.2 km depth (Hickman *et al.*, 2005).

We observed variations in the magnitude of fault healing along fault strike and with depth. Larger decreases in travel time (larger increase in seismic wave velocity) were measured for repeated aftershocks occurring beneath Middle Mountain (Fig. 8), where the maximum slips were found in the 2004 Parkfield **M** 6.0 earthquake. The travel-time changes increase with focal depth of aftershocks at between 3 km and 7 km depth, indicating that healing occurs on the fault to at least ~7 km depth. Because we have captured healing for only one cluster of repeated aftershocks at depth below ~7 km in this study, we lack constraints on the healing magnitude for the deeper portion of the fault zone. However, the repeated events in cluster 11 at the depth of ~9.2 km show larger time delays than those at shallower depths (Fig. 7).

The net coseismic decrease in shear-wave velocity

within the fault zone at depths above ~7 km caused by this **M** 6.0 event is thus estimated to be at least ~2.5%, accounting for the measurements of travel-time increase (seismic velocity decrease) of ~1.25% for repeated shots in the fall of 2002 and 28 December 2004, and travel-time decrease (velocity increase) of ~1.1% for repeated aftershocks in the 3 months starting a week after the mainshock on 28 September 2004. In contrast, the changes in shear velocity in surrounding rocks were smaller than ~0.5%. Because we have no data from the array site in the first week after the mainshock, we do not have information about the earliest stage of fault healing. However, Rubinstein and Beroza (2005) observed significant travel-time delays caused by the 2004 **M** 6.0 Parkfield earthquake at the seismic network stations for repeated earthquakes occurring at depths of ~3 km near the SAFOD drilling site before and after the 2004 **M** 6.0 earthquake. They measured travel-time decreases exceeding ~25 msec in *S* coda for the repeated SAFOD target events occurring on 21 and 23 October 2003, approximately one year before the **M** 6.0 earthquake, and on 28 September 2004 immediately after the mainshock at borehole station PMM of the Parkfield seismic network (Fig. 1a), located ~200 m from the SAF main trace at ~5 km southwest of the SAFOD site. They also observed direct *S*-wave travel-time delays up to 7 ms to many of the surface stations, but much smaller delays at borehole stations in the Parkfield area. They attribute the time delays to cracks opened during the strong shaking of the **M** 6.0 Parkfield earthquake at depths shallower than 100–300 m. Crack opening is likely favored at shallow depths, with soft rock and lower confining crustal stress in a broad distance range from the epicenter due to strong ground motion. However, stations of our dense array were located much closer to the fault than network stations. The data presented here from the shots and aftershocks located on or close to the fault mainly document the changes within the fault zone rather than the changes in surrounding rocks. We interpret the observed velocity decrease within the fault zone as mainly due to crack opening caused by the dynamic rupture of the latest **M** 6.0 earthquake. Shaking-induced weakening may also effect the rupture propagation because the pre-existing weak, low-impedance fault zone is susceptible to damage (Fialko *et al.*, 2002; Vidale and Li, 2003). Calculation for a ~2.5% decrease in velocity revealed that the apparent crack density within the rupture zone increased by ~0.035, which caused ~5% decrease in shear rigidity of the fault-zone rock during dynamic rupture of the 2004 **M** 6.0 Parkfield earthquake. The subsequent 1.1% increase in *S* velocity during the 3 months starting a week after the mainshock suggests the apparent crack density within the rupture zone decreased by 0.016, causing a ~2.2% increase in shear rigidity of the fault-zone rock during the early postmainshock period.

During the fault healing, the reduction of crack density may be controlled by a combination of mechanical and chemical processes on the active fault. Fault healing may be affected by time-dependent frictional strengthening (Vidale *et al.*, 1994; Marone, 1998; Schaff and Beroza, 2004), rheological fluid variations or changes in the state of stress (Blanpied *et al.*, 1992; Dodge and Beroza, 1997; Peltzer *et al.*, 1998), cementation, recrystallization, pressure solution, crack sealing and grain contact welding (Hickman and Evans, 1992; Olsen *et al.*, 1998; Sleep *et al.*, 2000; Morgan, 2004), and the fault-normal compaction of the rupture zone (Massonnet *et al.*, 1996; Boettcher and Marone, 2004), as well as chemical healing from mineralogical lithification of gouge materials over longer time periods at seismogenic depth (Angevine *et al.*, 1982). In addition, the "crack dilatancy" mechanisms (Nur, 1972) associated with the earthquake are likely to operate for coseismic fault damage and postmainshock healing even if other processes are active too. The stress-related temporal changes in seismic velocity caused by the 1989 Loma Prieta, California, earthquake have been reported (Dodge and Beroza, 1997; Schaff and Beroza, 2004). Baisch and Bokelmann (2001) suggest that coseismic deformation caused by this earthquake might lead to crack opening either by localizations of shear stress or by elevated pore-fluid pressure. Concentrated deformation at low-strength fault zones may help to cause damage. After the earthquake, relaxational processes such as crack healing, fluid diffusion, and postseismic deformation caused the cracks to close again and can be approximated by a logarithmic recovery rate. As rocks heal, a contribution can be from either continued right-lateral deformation due to the regional stress field that dominated the coseismic displacements, or fault-normal compression owing to a reduction in crack volume. The variation in apparent crack density inferred by seismic velocity measurements reflects changes in either crack volume or rearrangement of aspect ratio caused by the earthquake. We conclude that cracks that opened during the mainshock closed soon thereafter. This is consistent with our interpretation of the soft, low-velocity fault-zone waveguide on the SAF as being at least partially weakened in the 2004 **M** 6.0 mainshock, but with possible significant cumulative effects as well.

The temporal changes in crack-induced anisotropy near the Nojima fault that ruptured in the 1995 *M* 7.1 Kobe earthquake have been observed in shear-wave splitting (Tadokoro *et al.*, 1999; Ikuta and Yamaoka, 2004). However, there was no clear change in shear-wave splitting anisotropy after the 1999 Hector Mine earthquake (Cochran *et al.*, 2003). In addition, Cochran *et al.* (2005) also observed no clear changes in shear-wave splitting parameters along the SAF associated with the 2004 Parkfield earthquake, using some of the same seismic array data as presented here, suggesting that the shear-wave splitting may be not sensitive enough to detect small changes in crack density because the velocity change influences both the fast and slow orthogonally polarized shear waves. However, they see strong fault-parallel alignment in the polarization direction of the fast *S* wave within a 100- to 200-m-wide zone along the strike of the SAF that overlaps with the region of greatest velocity reductions reported here.

We also note that the ratio of travel-time changes for *P* to *S* waves is 0.57 within the rupture zone and ~0.65 in the surrounding rocks (Fig. 3d), suggesting that cracks within the fault zone are more wet than those out of the zone at shallow depths, according to equations for the elastic moduli of the medium with cracks (Garbin and Knopoff, 1975). This may be due to the higher permeability owing to higher porosity within the damaged fault zone than in the surrounding rocks, even though every crack includes a similar fraction of fluids. High permeability and low strength have been measured in a damage zone centered at the main trace of the Nojima fault in the 1995 Kobe earthquake (Lockner *et al.*, 2000). High-pressure water is coming up from depth, and the highly fractured fault zone acts as a fluid channel.

Our observations of fault-zone damage and healing associated with the latest **M** 6.0 Parkfield earthquake are in general consistent with the model of velocity as a function of time owing to damage and healing for the Lander and Hector Mine earthquakes (Vidale and Li, 2003). However, the magnitude of damage and healing observed on the SAF is smaller than those on the Landers and Hector Mine rupture zones, probably related to the magnitudes of earthquake, slip, stress drop, pore pressure, and rock type.

Acknowledgments

This study was supported by NSF/EarthScope Grant EAR-0342277, USGS Grant NEHRP20060160, and partially by the SCEC. Special thanks to S. Hickman, W. Ellsworth, and M. Zoback of SAFOD PIs for their coordination in our experiments for seismic characterization of the SAFOD drilling. We acknowledge J. Varian, G. Varian, G. Work, and B. Mosby for permissions to conduct our experiment on their lands, and the IRIS for the use of PASSCAL instruments. We are grateful to P. Malin, C. Thurber, S. Roecker, M. Rymer, R. Catchings, A. Snyder, R. Russell, L. Powell, B. Nadeau, N. Boness, D. McPhee, and F. Niu for their collaborations in our research at Parkfield. We thank associate editor Ramon Arrowsmith, reviewer Norm Sleep, and an anonymous reviewer for their helpful suggestions and comments on the manuscript. This research was supported by the Southern California Earthquake Center. SCEC is funded by NSF Cooperative Agreement EAR-0106924 and USGS Cooperative Agreement 02HQAG0008. The SCEC contribution number for this paper is 924.

References

Aki, K. (1984). Asperities, barriers, characteristic earthquakes, and strong motion prediction, *J. Geophys. Res.* **89,** 5867–5872.

Angevine, C. L., D. L. Turcotte, and M. D. Furnish (1982). Pressure solution lithification as a mechanism for the stick-slip behavior of faults, *Tectonics* **1,** 151–160.

Baisch, S., and G. H. R. Bokelmann (2001). Seismic waveform attributes before and after the Loma Prieta earthquake: scattering change near the earthquake and temporal recovery, *J. Geophys. Res.* **106,** 16,323–16,337.

Blanpied, M. L., D. A. Lockner, and J. D. Byerlee (1992). An earthquake mechanism based on rapid sealing of faults, *Nature* **359,** 574–576.

Boettcher, M. S., and C. Marone (2004). Effects of normal stress variation on the strength and stability of creeping faults, *J. Geophys. Res.* **109,** B03406, dioi 10.1029/2003JB002824.

Byerlee, J. (1990). Friction, overpressure and fault-normal compression, *Geophys. Res. Lett.* **17,** 2109–2112.

Chester, F. M., J. P. Evans, and R. L. Biegel (1993). Internal structure and weakening mechanisms of the San Andreas fault, *J. Geophys. Res.* **98,** 771–786.

Cochran, S. E., J. E. Vidale, and Y. G. Li (2003). Near-fault anisotropy following the Hector Mine earthquake, *J. Geophys. Res.* **108,** B9, 2436–2447, ESE 11.

Cochran, S. E., Y. G. Li, and J. E. Vidale (2006). Anisotropy in the shallow crust observed around the San Andreas fault before and after the 2004 **M** 6.0 Parkfield earthquake, *Bull. Seism. Soc. Am.* **96,** no. 4B, S364–S375.

Dieterich, J. H. (1978). Time-dependent friction and the mechanics of strike-slip. *Pure Appl. Geophys.* **116,** 790–806.

Dodge, D., and G. C. Beroza (1997). Source array analysis of coda waves near the 1989 Loma Prieta, California, mainshock: implications for the mechanism of coseismic velocity changes, *J. Geophys. Res.* **102,** 24,437–24,458.

Eberhart-Phillips, D., and A. J. Michael (1993). Three-dimensional velocity structure, seismicity, and fault structure in Parkfield region, central California, *J. Geophys. Res.* **98,** 15,737–15,758.

Fialko, Y., D. Sandwell, D. Agnew, M. Simons, P. Shearer, and B. Minster (2002). Deformations on nearby faults induced by the 1999 Hector Mine earthquake, *Science* **297,** 1858–1862.

Garbin, H. D., and L. Knopoff (1975). Elastic moduli of a medium with liquid-filled cracks, *Quart. Appl. Math.* **32,** 301–303.

Hickman, S. H., and B. Evans (1992). Growth of grain contacts in halite by solution-transfer: implications for diagenesis, lithification, and strength recovery, in *Fault Mechanics and Transport Properties of Rocks*, Academic, San Diego, 253–280.

Hickman, S. H., M. D. Zoback, and W. L. Ellsworth (2005). Structure and Composition of the San Andreas fault zone at Parkfield: initial results from SAFOD phase 1 and 2, *EOS Trans Am Geophys Union* **83,** no. 47, 237.

Ikuta, R., and K. Yamaoka (2004). Temporal variation in the shear wave anisotropy detected using the accurately controlled routinely operated signal system (ACROSS), *J. Geophys. Res.* **109,** B09305, doi 10.1029/2003JB002901.

Kanamori, H. (1994). Mechanics of earthquakes, *Annu. Rev. Earth Planet. Sci.* **22,** 207–237.

Korneev, V. A., R. M. Nadeau, and T. V. McEvilly (2003). Seismological studies at Parkfield IX: fault-zone imaging using guided wave attenuation, *Bull. Seism. Soc. Am.* **80,** 1245–1271.

Langbein, J., R. Bocherdt, D. Dreger, J. Fletcher, J. L. Hardbeck, M. Hellweg, C. Ji, M. Johnston, J. R. Murray, R. Nadeau, M. J. Rymer, and J. A. Trieman (2005). Preliminary report on the 28 September 2004, *M* 6.0 Parkfield, California, earthquake, *Seism. Res. Lett.* **76,** no. 1, 10–26.

Lees, J. M., and P. E. Malin (1990). Tomographic images of *P*-wave velocity variation at Parkfield, California, *J. Geophys. Res.* **95,** 21,793–21,804.

Li, Y. G., and J. E. Vidale (2001). Healing of the shallow fault zone from 1994–1998 after the 1992 *M* 7.5 Landers, California, earthquake, *Geophys. Res. Lett.* **28,** 2999–3002.

Li, Y. G., W. L. Ellsworth, C. H. Thurber, P. E. Malin, and K. Aki (1997). Observations of fault-zone trapped waves excited by explosions at the San Andreas fault, central California, *Bull. Seism. Soc. Am.* **87,** 210–221.

Li, Y. G., P. C. Leary, K. Aki, and P. E. Malin (1990). Seismic trapped modes in Oroville and San Andreas fault zones, *Science* **249,** 763–766.

Li, Y. G., J. E. Vidale, K. Aki, F. Xu, and T. Burdette (1998). Evidence of shallow fault zone strengthening after the 1992 *M* 7.5 Landers, California, earthquake, *Science* **279,** 217–219.

Li, Y. G., J. E. Vidale, and S. E. Cochran (2004). Low-velocity damaged structure on the San Andreas fault at Parkfield from fault-zone trapped waves, *Geophys. Res. Lett.* **31,** L12S06, 1–5.

Li, Y. G., J. E. Vidale, S. M. Day, D. D. Oglesby, and E. Cochran (2003). Post-seismic fault healing on the 1999 *M* 7.1 Hector Mine, California, earthquake, *Bull. Seism. Soc. Am.* **93,** 854–869.

Lockner, D. A., H. Naka, H. Tanaka, H. Ito, and R. Ikeda (2000). Permeability and strength of core samples from the Nojima fault of the 1995 Kobe earthquake, in *Proc. of the International Workshop on the Nojima Fault Core and Borehole Data Analysis,* Tsukuba, Japan, 22–23 November 1999, H. Ito, K. Fujimoto, H. Tanaka, and D. A. Lockner (Editors), USGS Open-File Report 00-129, 147–152.

Malin, P. E., E. Shalev, H. Balven, and C. L. Kenedi (2006). New fault structure on the San Andreas fault at SAFOD from P-wave tomography and fault guided waves mapping, *Geophys. Res. Lett.* **33,** (in press).

Marone, C. (1998). The effect of loading rate on static friction and the rate of fault healing during the earthquake cycle, *Nature* **391,** 69–72.

Marone, C., J. E. Vidale, and W. L. Ellsworth (1995). Fault healing inferred from time dependent variations in source properties of repeating earthquakes, *Geophys. Res. Lett.* **22,** 3095–3098.

Massonnet, D., W. Thatcher, and H. Vadon (1996). Detection of postseismic fault-zone collapse following the Landers earthquake, *Nature* **382,** 612–616.

Michelini, A., and T. V. McEvilly (1991). Seismological studies at Parkfield, I: Simultaneous inversion for velocity structure and hypocenters using cubic B-splines parameterization, *Bull. Seism. Soc. Am.* **81,** 524–552.

Mooney, W. D., and A. Ginzburg (1986). Seismic measurements of the internal properties of fault zones, *Pure Appl. Geophys.* **124,** 141–157.

Morgan, J. K. (2004). Particle dynamics simulations of rate- and state-dependent frictional sliding of granular gouge, *Pure Appl. Geophys.* **161,** 1877–1891.

Niu, F. L., P. G. Silver, R. M. Nadeau, and T. V. McEvilly (2003). Stress-induced migration of seismic scatters associated with 1993 Parkfield aseismic transient event, *Nature* **426,** 544–548.

Nur, A., and A. Dilatancy (1972). Pore fluid and premonitory variations of t_s/t_p travel times, *Bull. Seism. Soc. Am.* **62,** 1217–1222.

O'Connell, R. J., and B. Budiansky (1974). Seismic velocities in dry and saturated cracked solids, *J. Geophys. Res.* **79,** 5412–5426.

Olsen, M., C. H. Scholz, and A. Leger (1998). Healing and sealing of a simulated fault gouge under hydrothermal conditions for fault healing, *J. Geophys. Res.* **103,** 7421–7430.

Peltzer, G., P. Rosen, F. Rogez, and K. Hudnut (1998). Poroelastic rebound along the Landers 1992 earthquake surface rupture, *J. Geophys. Res.* **103,** 30,131–30,145.

Rice, J. R. (1980). The mechanics of earthquake rupture, in *Physics of the Earth's Interior*, A. M. Dziewonski and B. Boschi (Editors), North-Holland, Amsterdam, 555–649.

Rice, J. R. (1992). Fault stress states, pore pressure distributions, and the weakness of the San Andreas fault, in *Fault Mechanics and Transport Properties of Rocks,* B. Evans and T.-F. Wong (Editors), Academic, San Diego, 475–503.

Richardson, E., and C. Marone (1999), Effects of normal stress vibrations on frictional healing, *J. Geophys. Res.* **104,** 28,859–28,878.

Roecker, S., C. H. Thurber, and D. McPhee (2004). Joint inversion of gravity and arrival time data from Parkfield: new constraints on structure and hypocenter locations near the SAFOD drill site, *Geophys. Res. Lett.* **31,** 1–4.

Rubinstein, J., and G. C. Beroza (2005). Depth constrain on nonlinear strong ground motion from the 2004 Parkfield earthquake, Seism. Res. Lett. **32,** L14313, doi 10.1029/2005GL023189.

Schaff, D. P., and G. C. Beroza (2004). Coseismic and postseismic velocity changes measured by repeating earthquakes, *J. Geophys. Res.* **109,** B10302, doi 10.1029/2004JB003011.

Scholz, C. H. (1990). *The Mechanics of Earthquakes and Faulting,* Cambridge Univ. Press, New York.

Shalev, E., and P. E. Malin (2005). Fault-zone guided waves observations in the SAFOD drill hole, in EarthScope National Annual Meeting Proceedings, 228.

Sleep, N. H., E. Richardson, and C. Marone (2000). Physics of friction and strain rate localization in synthetic fault gouge, *J. Geophys. Res.* **105,** 25,875–25,890.

Snieder, R. A., A. Gret, H. Douma, and J. Scales (2002). Coda wave interferometry for estimating nonlinear behavior in seismic velocity, *Science* **295,** 2253–2255.

Tadokoro, K, M. Ando, and Y. Umeda (1999). *S*-wave splitting in the aftershock region of the 1995 Hyogo-ken Nanbu earthquake, *J. Geophys. Res.* **104,** 981–991.

Thurber, C. H., S. Roecker, W. Ellsworth, Y. Chen, W. Lutter, and R. Sessions (1997). Two-dimensional seismic image of the San Andreas fault in the northern Gabilan Range, central California: evidence for fluids in the fault zone, *Geophys. Res. Lett.* **24,** 1591–1594.

Thurber, C., S. Roecker, K. Roberts, M. Gold, L. Powell, and K. Rittger (2003). Earthquake location and three-dimensional fault zone structure along the creeping section of the San Andreas fault near Parkfield, California: preparing for SAFOD, *Geophys. Res. Lett.* **30,** 1112–1115.

Unsworth, M., P. Malin, G. Egbert, and J. Booker (1997). Internal structure of the San Andreas fault at Parkfield, California, *Geology* 356–362.

Vidale, J. E., and Y. G. Li (2003). Damage to the shallow Landers fault from the nearby Hector Mine earthquake, *Nature* **421,** 524–526.

Vidale, J. E., W. L. Ellsworth, A. Cole, and C. Marone (1994). Rupture variation with recurrence interval in eighteen cycles of a small earthquake, *Nature* **368,** 624–626.

Yasuhara, H., C. Marone, and D. Ellsworth (2005). Fault zone restrengthening and frictional healing: the role of pressure solution, *J. Geophys. Res.* **110,** B06310, doi 10.1029/2004JB003327 2003.

Department of Earth Sciences
University of Southern California
Los Angeles, California 90089-0740
ygli@usc.edu
(Y.G.L., P.C.)

Institute of Geophysics and Planetary Physics
Scripps Institution of Oceanography
La Jolla, California, 92093-0225
(E.S.C.)

Institute of Geophysics and Planetary Physics
University of California, Los Angeles
Los Angeles, California 90095
(J.E.V.)

U.S. Geological Survey, MS 977
345 Middlefield Road
Menlo Park, California 94025
(T.B.)

Manuscript received 24 August 2005.